Alq J Sci. 2026;2(10):938-944
https://doi.org/10.69667/ajs.261005

Alqalam Journal of Science
مجلـــة القلم للعلـوم
https://alqalam.utripoli.edu.ly/index.php/AR

Original article

Monte Carlo Simulation Study on Enamine Derivatives as Potential Corrosion Inhibitors for Mild Steel on the Fe(110) Interface

Sali Ahmed[1]*, Abdalhamid Alarafi[2]

[1]Department of Chemistry, Faculty of Arts and Sciences, University of Benghazi, Qamiinis, Libya
[2]Department of Chemistry, Faculty of Arts and Sciences, University of Benghazi, Al-Abyar, Libya
Email. Sali.abdelal@uob.edu.ly

Abstract
A thorough understanding of molecular-level processes at the metal-electrolyte boundary is necessary for the design of highly effective, environmentally friendly organic inhibitors. The interfacial adsorption thermodynamics, spatial orientation mechanisms, and corrosion inhibition efficacy of seven enamine derivatives (L1–L7) on the Fe(110) substrate were examined in this work using Advanced Monte Carlo (MC) simulations. Highly negative adsorption energies (Eads) ranging from -551.33 to -954.50 kJ mol-1 were shown by simulated annealing protocols (30,000 steps over three cycles) with the COMPASSIII force field, indicating energetically favorable adsorption and strong inhibitor–surface interactions. The hierarchical order is strictly followed by the computational binding affinity: L5 > L7 > L4 > L6 >> L1 > L3 > L2. Important mechanistic insights into molecular spatial adaptation were obtained by deconvolution of Eads into rigid adsorption (Erigid) and structural deformation (Edeformation) components. Strong charge-transfer interactions involving heteroatoms (N, O), delocalized π-electrons, and unoccupied Fe d-orbitals are displayed by the best-performing cluster (L4–L7, Eads < -918 kJ mol-1); side-view analysis showed different equilibrium separation distances (deq) for L2 and L7. Interestingly, L7 adopts a parallel aromatic alignment to maximize surface coverage footprint, thereby overcoming a severe geometric deformation penalty (-637.14 kJ mol-1). Stable adsorption configurations derived from the Monte Carlo calculations are consistent with the strong numerical agreement between Eads and the differential adsorption energy (dEads/dNi). These findings support the idea that enamine architectures, particularly L5 and L7, are good candidates for cutting-edge corrosion prevention techniques for mild steel.
Keywords: Enamine Scaffolds, Corrosion Inhibition, Monte Carlo Simulation, Fe(110) Interface.

Introduction

When carbonyl compounds react with amine nucleophiles to form enamines and enols, a crucial class of structural analogs, cyclic secondary amines like pyrrolidine, piperidine, and morpholine serve as traditional precursor bases [1]. Wittig first used the term "enamine" in 1927 to highlight the conceptual and reactivity similarities to enols [6], despite Mannich having published the first foundational synthesis of enamines nine years earlier [2], with historical roots dating back to 1884 [3–5]. The fundamental chemical scope and synthetic significance of enamine–electrolyte systems were significantly altered by Stork's seminal work in 1954 [7–10]. In the years that followed, enamine chemistry saw significant scientific advancement [11]. Up until the early 1970s, enamines played a unique role as neutral enolate synthetic equivalents; later, they shared this role with silylated enol ethers [12–19]. The primary source of their synthetic utility is their intrinsic nucleophilicity toward a variety of electrophilic species, including Michael acceptors [24–25], electron-deficient dienes functioning as π4 cycloaddition partners [21–23], and acceptor-activated aryl halides [20]. Furthermore, their dynamic covalent and non-covalent interactions facilitate the formation of adaptive supramolecular structures and constitutional exchange networks [26–43].

At the electronic scale, the enamine structure exhibits an electron-rich π-system, which is defined by strong p–π conjugation between the nitrogen's lone electron pair and the nearby ethylenic C=C double bond. Extensive cyclic voltammetry studies have examined the electro-oxidation properties and redox pathways of secondary enamines derived from primary amines and β-keto carbonyl compounds [44]. In addition to their synthetic adaptability and electrochemical qualities, these scaffolds with conjugated heteroatoms exhibit a broad range of bioactivities, including antibacterial, antifungal, antiviral, anti-inflammatory, and anticancer effects [45].

Although a lot of research has been done on the synthesis processes, electrochemical behaviors, and biological applications of enamine derivatives, little is known about their potential as corrosion inhibitors at the metal-solution interface. This study investigates the corrosion inhibition characteristics of seven enamine derivatives (L1–L7) that have been previously reported [44]. These derivatives have electron-rich frameworks, heteroatoms (N, O), and conjugated π-orbitals, which make them suitable for donor–acceptor interactions with the unoccupied d-orbitals of surface iron atoms. Using Advanced Monte Carlo (MC) simulations, we quantitatively examine their binding energies, equilibrium spatial configurations, and adsorption orientations on the Fe(110) crystal surface. By methodically breaking down the components of adsorption energy (Eads, Erigid, Edeformation), this study provides a thorough molecular-level understanding of the process by which a protective film forms to shield mild steel from corrosion.

Copyright *Author (s) 2026. Distributed under Creative Commons CC-BY 4.0*
Received: *01-08-2026 -* ***Accepted:*** *30-09-2026 -* ***Published:*** *08-10-2026*

Alq J Sci. 2026;2(10):938-944
https://doi.org/10.69667/ajs.261005
Alqalam Journal of Science
مجلـــة القلم للعلـوم
https://alqalam.utripoli.edu.ly/index.php/AR

Computational Details

Molecular Models and Structural Optimization

To investigate their interfacial adsorption mechanisms and spatial arrangements on the iron surface, seven previously synthesized enamine derivatives (L1–L7) were selected as target corrosion inhibitors [44]. The two-dimensional (2D) molecular configurations of the compounds being studied are shown in Figure 1. All inhibitor geometries were fully optimized and energy-minimized using the COMPASSIII force field prior to surface mounting and adsorption simulations.

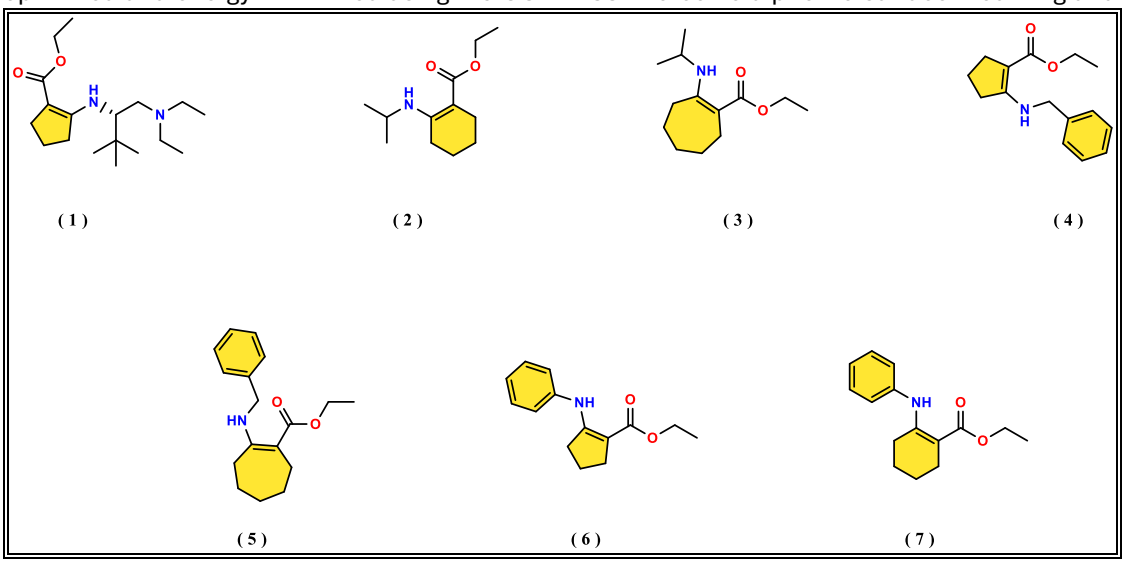


Figure 1: 2D chemical structures of the studied enamine derivatives (L1 – L7).

Substrate Construction and Monte Carlo Simulation Protocols

The Adsorption Locator module of BIOVIA Materials Studio 2023 (Dassault Systèmes) was used to perform interfacial Monte Carlo (MC) simulations. Each optimized enamine derivative (L1–L7) was added separately as a sorbate to the Fe(110) surface, which functioned as the adsorbent substrate. Five atomic layers totaling 180 Fe atoms made up the Fe(110) substrate model. A 6 × 6 × 1 supercell was used to create the Fe(110) surface. The simulation cell's dimensions were approximately a = 14.894 Å, b = 14.894 Å, and c = 38.107 Å. Its angles were α = 90°, β = 90°, and γ = 70.529°. A vacuum space of about 30.0 Å separated the five-layer Fe(110) slab, which contained 36 Fe atoms in each layer, from its periodic image. A P1 three-dimensional periodic simulation cell was used to create the model.

Instead of limiting the inhibitor molecules to a particular adsorption orientation, possible adsorption configurations were examined using translational, rotational, and regrowth On the Fe(110) surface, Monte Carlo moves are used to identify advantageous adsorption geometries. The COMPASSIII force field (Version 1.2) was used for the computations, and atomic partial charges were assigned according to the force-field parameters. Throughout the adsorption calculations, geometry optimization was enabled. The Monte Carlo step sizes were automatically adjusted during the automatic mode of simulated annealing. Three thermal cycles, each with 10,000 steps, and 100,000 loading steps were used in the computation. An atom-based summation method using cubic-spline truncation was used to evaluate electrostatic and van der Waals forces. A cutoff distance of 18.5 Å, a spline width of 1.0 Å, and a buffer width of 0.5 Å were used for both interaction terms. Each of the seven inhibitor molecules (L1–L7) was simulated separately on the Fe(110) surface using the same Monte Carlo simulation protocol and computational parameters. No user-specified numerical convergence tolerance was used; instead, the Adsorption Locator automatically controlled the simulated-annealing process, modifying the Monte Carlo step sizes on its own. No temperature range was set by the user because Adsorption Locator automatically controlled the annealing temperature schedule.

Thermodynamic Energy Calculations

The following thermodynamic definitions were used to determine the energetic parameters describing the minimum-energy states on the Fe(110) surface:[46] .

$$E_{substrate + adsorbate} = E_{total}$$
$$E_{rigid} + E_{def} = E_{ads}$$

where E_{ads} is the total adsorption energy, E_{def} is the deformation energy associated with structural relaxation during adsorption, E_{rigid} is the energy released when the unrelaxed adsorbate binds to the substrate, and E_{total} is the mean total energy of the substrate-inhibitor system [46]. The comparative stability of the obtained adsorption configurations was

Copyright *Author (s) 2026. Distributed under Creative Commons CC-BY 4.0*
Received: *01-08-2026 -* ***Accepted:*** *30-09-2026 -* ***Published:*** *08-10-2026*

Alq J Sci. 2026;2(10):938-944
https://doi.org/10.69667/ajs.261005
Alqalam Journal of Science
مجلـــة القلم للعلـوم
https://alqalam.utripoli.edu.ly/index.php/AR

assessed using the differential adsorption energy (dEads/dNi), which represents the energy variation associated with the addition or removal of an adsorbate component.

Results and Discussion

Adsorption Energetics and Interfacial Behavior on Fe(110)

The Adsorption Locator module was used in Monte Carlo (MC) simulations to assess the binding affinity and inhibition efficacy of the synthesized enamine derivatives (L1–L7) on the Fe(110) substrate. The adsorption configurations with the highest thermodynamic favorability and the global energy minimum were found. Table 1 displays the energy values obtained: Total Energy (Etotal), Adsorption Energy (Eads), Rigid Adsorption Energy (Erigid), Deformation Energy (Edeformation), and Differential Adsorption Energy (dEads/dNi).

Table 1: The output energies calculated by Monte Carlo simulation for (L1-L7) on Fe(110)

Inhibitor	Total energy (kJ mol^{-1})	Adsorption energy (kJ mol^{-1})	Rigid adsorption energy (kJ mol^{-1})	Deformation energy (kJ mol^{-1})	$(dE_{ads}/dNi)\ (kJ\ mol^{-1})$
L1	-551.02	-631.54	-391.15	-240.39	−631.54
L2	−521.11	−551.33	−271.45	−279.88	−551.33
L3	−593.23	−552.64	−344.22	−208.41	−552.64
L4	−438.84	−944.02	−401.75	−542.27	−944.02
L5	−476.28	−954.50	−419.87	−534.63	−954.50
L6	−440.94	−918.81	−349.12	−569.68	−918.81
L7	−450.25	−948.93	−311.83	−637.14	−948.93

For every inhibitor under investigation, the computed adsorption energies (Eads) ranged from -551.33 to -954.50 kJ mol-1. A stronger interaction between the inhibitor and the surface and a more energetically favorable adsorption process are indicated by a lower Eads value. It also suggests that the inhibitor can more effectively form a protective barrier layer. By acting as a barrier, this layer shields the iron sites from dangerous environmental substances like (H2O, Cl-, H3O+). The adsorption strength and theoretical inhibition performance on the Fe(110) crystal plane appear in the following order when looking at the numbers in Table 1:
L5 > L7 > L4 > L6 >> L1 > L3 > L2

Comparative Performance Analysis

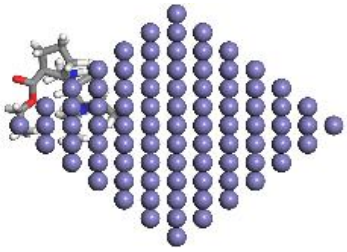
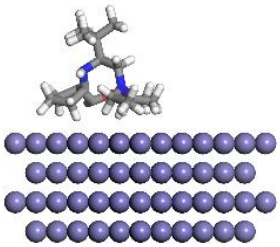
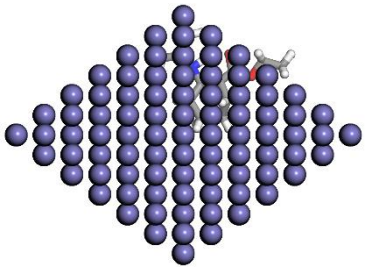
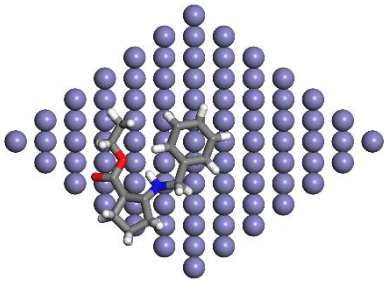
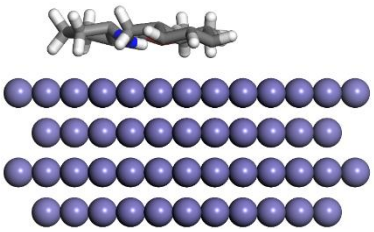
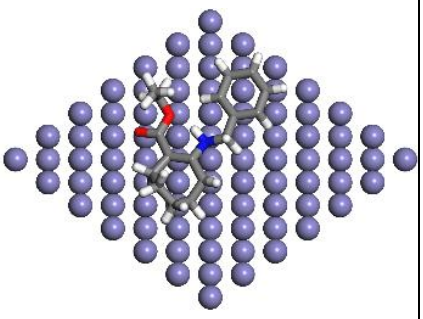
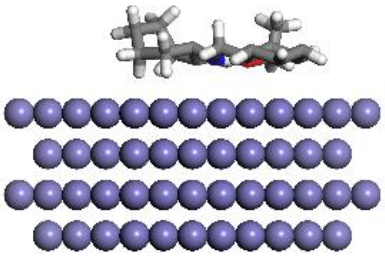
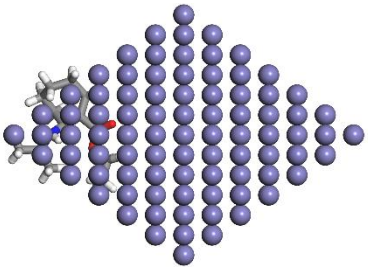
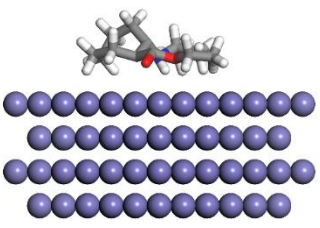
1. High-Performance Cluster (L4, L5, L6, L7): The adsorption energy values of compounds L4, L5, L6, and L7 were remarkable, surpassing -918 kJ mol-1. L5 had the lowest adsorption energy (Eads = -954.50 kJ mol-1), followed closely by L7 (Eads = -948.93 kJ mol-1), L4 (Eads = -944.02 kJ mol-1), and L6 (Eads = -918.81 kJ mol-1). The cooperative interaction between electron-donating heteroatoms (N, O) and the delocalized π-electron framework of the enamine configuration is responsible for this group's exceptional binding strengths. With the unoccupied d-orbitals of the iron atoms on the surface, these active sites promote strong charge-transfer/donor-acceptor interactions.
2. Moderate-Performance Cluster (L1, L2, L3): The adsorption energies of inhibitors L1, L2, and L3 were lower, ranging from -551.33 kJ mol-1 to -631.54 kJ mol-1. The less negative Eads values indicate that the inhibitor–surface interactions are weaker than those of the high-performance cluster, even though their adsorption is still energetically favorable.

Deconvolution of Adsorption Energy and Conformational Spatial Orientations

A deeper structural understanding of the interfacial behavior can be obtained by dissecting Eads into its rigid and deformation segments using the mathematical model developed in the computational methodology (Eads = Erigid + Edeformation). The global minimum adsorption configurations of enamine derivatives (L1–L7) on the Fe(110) surface, obtained from Monte Carlo simulations, are displayed in both Top views (A) and Side views (B) in Figure 2.

Copyright *Author (s) 2026. Distributed under Creative Commons CC-BY 4.0*
Received: *01-08-2026 -* ***Accepted:*** *30-09-2026 -* ***Published:*** *08-10-2026*

Alq J Sci. 2026;2(10):938-944
https://doi.org/10.69667/ajs.261005
Alqalam Journal of Science
مجلـــة القلم للعلـوم
https://alqalam.utripoli.edu.ly/index.php/AR

Ligands	(A)	(B)
1		
2		
3		
4		
5		

Copyright *Author (s) 2026. Distributed under Creative Commons CC-BY 4.0*
Received: *01-08-2026 -* ***Accepted:*** *30-09-2026 -* ***Published:*** *08-10-2026*

Alq J Sci. 2026;2(10):938-944
https://doi.org/10.69667/ajs.261005
Alqalam Journal of Science
مجلـــة القلم للعلـوم
https://alqalam.utripoli.edu.ly/index.php/AR

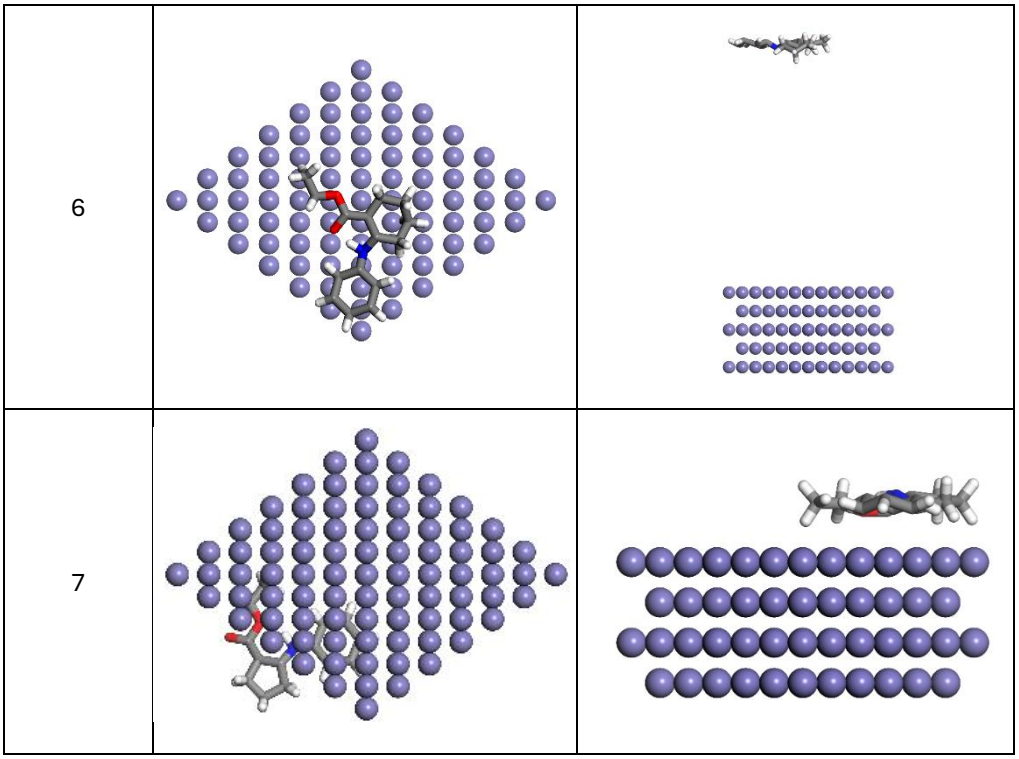


Figure 2: Global minimum adsorption configurations of enamine derivatives (L1–L7) on the Fe(110) surface obtained from Monte Carlo simulations: (A) Top views and (B) Side views

- **Rigid Adsorption Energy (E_{rigid}):** indicates the binding interaction that is unrelaxed prior to any geometric distortion. L5 (-419.87 kJ mol-1) had the highest Erigid, followed by L4 (-401.75 kJ mol-1) and L1 (-391.15 kJ mol-1). This demonstrates the early adsorption stage's strong initial electrostatic and dispersion attraction.
- **Origin of Equilibrium Separation Distance in L2 and L7:** he existence of a particular equilibrium separation distance (deq) for inhibitors L2 and L7, while compounds L1, L3, L4, L5, and L6 adsorb closer to the surface, is a significant structural detail from the side views of the adsorbed configurations (Figure 2B). There are two basic mechanisms underlying this behavior:
  1. L2 (Weak Binding Affinity & Steric Non-Planarity): Throughout the entire series, inhibitor L2 exhibits the lowest net adsorption energy (Eads = -551.33 kJ mol-1) and rigid adsorption energy (Erigid = -271.45 kJ mol-1). In order to prevent short-range electron-cloud repulsions with the surface, the non-planar nature of its non-aromatic/saturated substituents and the lack of strong attractive interactions result in an increased separation distance.
  2. L7 (Bulky Steric Hindrance & Exceptional Deformation Energy): On the other hand, L7 has the highest deformation energy of any compound (Edeformation = -637.14 kJ mol-1). Significant steric hindrance is caused by the bulky substituent groups in L7. L7 undergoes considerable geometric distortion and realigns itself at an equilibrium separation distance (deq) in order to lower the overall system energy. However, its aromatic fragments and active donor centers remain parallel to the Fe(110) plane, thereby compensating for the deformation penalty and providing a very high adsorption energy (Eads = -948.93 kJ mol-1).

Differential Adsorption Energy:

The energy required to separate an adsorbate element from the metal surface is indicated by the differential adsorption energy (dEads/dNi). The calculated dEads/dNi values for each of the seven enamine compounds matched their total Eads values (e.g., -954.50 kJ mol-1 for L5 and -948.93 kJ mol-1 for L7). Stable single-molecule adsorption configurations obtained from the Monte Carlo search are consistent with this numerical correlation.

Conclusion

In order to assess the adsorption thermodynamics, spatial arrangement mechanisms, and corrosion prevention capabilities of seven enamine derivatives (L1–L7) on the Fe(110) surface, this study successfully carried out Advanced Monte Carlo (MC) simulations. All of the investigated enamine compounds have noticeably high negative adsorption energies, ranging from -551.33 to -954.50 kJ mol-1, according to the computational analysis. The strongly negative adsorption energies support the

Copyright *Author (s) 2026. Distributed under Creative Commons CC-BY 4.0*
Received: *01-08-2026 -* ***Accepted:*** *30-09-2026 -* ***Published:*** *08-10-2026*

inhibitor molecules' potential efficacy in corrosion protection by indicating that the adsorption is energetically favorable and that there are strong interactions between them and the Fe(110) surface. L5 (-954.50 kJ mol-1) > L7 (-948.93 kJ mol-1) > L4 (-944.02 kJ mol-1) > L6 (-918.81 kJ mol-1) >> L1 (-631.54 kJ mol-1) > L3 (-552.64 kJ mol-1) > L2 (-551.33 kJ mol-1) is the predicted binding affinity and inhibition effectiveness on the Fe(110) surface. Important mechanistic insights into interfacial spatial modification were obtained through a more thorough structural dissection of the adsorption energy into its rigid (Erigid) and deformation (Edeformation) components. Compound L5 exhibited the highest intrinsic electronic affinity (Erigid = -419.87 kJ mol-1), while derivative L7's large substituent groups resulted in a significant geometric deformation penalty (Edeformation = -637.14 kJ mol-1). Importantly, spatial analyzes from both overhead and lateral perspectives demonstrated that L7 effectively lowers this deformation energy penalty by altering its active sites and aromatic framework at a specific equilibrium separation distance (deq) in a parallel alignment with the Fe(110) plane, increasing its surface coverage and overall binding strength. Strong synergistic charge-transfer interactions, in which electron-rich heteroatoms (N, O) and delocalized π-electron networks add charge density to the vacant d-orbitals of surface iron atoms, are responsible for the enhanced protection effectiveness displayed by the high-performance cluster (L4–L7, Eads < -918 kJ mol-1). Furthermore, stable adsorption configurations obtained from the Monte Carlo simulations are consistent with the strong numerical correlation between the net adsorption energy (Eads) and the differential adsorption energy (dEads/dNi). To sum up, these theoretical results show that enamine structures, especially derivatives L5 and L7, are extremely promising molecular frameworks for cutting-edge techniques to prevent mild steel corrosion.

References

1. Ouellette RJ, Rawn JD. Organic chemistry study guide: Key concepts, problems, and solutions. Amsterdam: Elsevier; 2015.
2. Wittig G, Blumenthal H. Über die Einwirkung von Ammoniak und Ammoniak-Derivaten auf o-Acetylaceto phenole. Ber Dtsch Chem Ges (A B Ser). 1927;60(5):1085-94
3. Mannich C, Davidsen H. Über einfache Enamine mit tertiär gebundenem Stickstoff. Ber Dtsch Chem Ges (A B Ser). 1936;69(9):2106-12.
4. Collie JN. Ueber die Einwirkung des Ammoniaks auf Acetessigester. Justus Liebigs Ann Chem. 1884;226(3):294-322.
5. Benary E. Über die Acylierung des β-Amino-crotonsäureesters und verwandter Verbindungen. Ber Dtsch Chem Ges. 1909;42(3):3912-25.
6. Robinson R. The C-alkylation of certain derivatives of ß-aminocrotonic acid. J Chem Soc. 1916;109:762-8.
7. Stork G, Terrell R, Szmuszkovicz J. A new synthesis of 2-alkyl and 2-acyl ketones. J Am Chem Soc. 1954;76(7):2029-30.
8. Stork G, Landesman HK. A new alkylation of carbonyl compounds. II. J Am Chem Soc. 1956;78(19):5128-9.
9. Stork G, Landesman HK. A new ring enlargement sequence. J Am Chem Soc. 1956;78(19):5129-30.
10. Stork G, Brizzolara A, Landesman H, Szmuszkovicz J, Terrell R. The enamine alkylation and acylation of carbonyl compounds. J Am Chem Soc. 1963;85(2):207-22.
11. Huang ZT, Wang MX. The Chemistry of Enamines. New York: Wiley; 1994. p. 1303.
12. Brownbridge P. Silyl enol ethers in Synthesis—part I. Synthesis. 1983;1983(1):1-28.
13. Brownbridge P. Silyl enol ethers in synthesis—part II. Synthesis. 1983;1983(2):85-104.
14. Reißig HU. Siliciumverbindungen in der organischen Synthese. Chem Unserer Zeit. 1984;18(2):46-54.
15. Reetz MT. Lewis-Säure-bewirkte α-Alkylierung von Carbonylverbindungen. Angew Chem. 1982;94(2):97-109.
16. Reetz MT. Lewis Acid Induced α-Alkylation of Carbonyl Compounds. Angew Chem Int Ed Engl. 1982;21(2):96 108.
17. Kaur P, Khatik GL, Nayak SK. A review on advances in organoborane chemistry: versatile tool in asymmetric synthesis. Curr Org Synth. 2017;14(5):665-82.
18. Reißig HU. Donor-acceptor-substituted cyclopropanes: Versatile building blocks in organic synthesis. In: de Meijere A, editor. Small ring compounds in organic synthesis III. Berlin: Springer; 1988. p. 73-135.
19. Mahrwald R. Diastereoselection in Lewis-acid-mediated aldol additions. Chem Rev. 1999;99(5):1095-120.
20. Whitesell JK, Whitesell MA. Alkylation of ketones and aldehydes via their nitrogen derivatives. Synthesis. 1983;1983(7):517-36.
21. Cook G. Enamines: synthesis, structure, and reactions. Boca Raton: CRC Press; 2017.
22. Shono T, Matsumura Y, Inoue K, Ohmizu H, Kashimura S. Electroorganic chemistry. 62. Reaction of iminium ion with nucleophile: A versatile synthesis of tetrahydroquinolines and julolidines. J Am Chem Soc. 1982;104(21):5753-7.
23. Murahashi SI, Naotao T, Nakato T. Convenient Method for the Construction of Quinoline Skeletons from N Methylarylamines via N-(t-Butyldioxymethyl) arylamines. Synlett. 1992;1992(10):835-6.
24. Chinchilla R. In: Bäckvall JE, editor. The chemistry of enamines. New York: Wiley; 1994.
25. Kuehne ME. The arylation of enamines. J Am Chem Soc. 1962;84(5):837-47.
26. Zhang Y, Qi Y, Ulrich S, Barboiu M, Ramström O. Dynamic covalent polymers for biomedical applications. Mater Chem Front. 2020;4(2):489-506.
27. Frei P, Hevey R, Ernst B. Dynamic combinatorial chemistry: a new methodology comes of age. Chem Eur J. 2019;25(1):60-73.
28. Zhang Y, Zhang Y, Ramström O. Dynamic covalent kinetic resolution. Catal Rev. 2020;62(1):66-95.
29. Orrillo AG, Escalante AM, Martinez-Amezaga M, Cabezudo I, Furlan RL. Molecular networks in dynamic multilevel systems. Chem Eur J. 2019;25(5):1118-27.
30. . Schaufelberger F, Timmer BJJ, Ramström O, Zhang W, Jin Y. Dynamic Covalent Chemistry: Principles, Reactions, and Applications. Weinheim: Wiley-VCH; 2017.
31. Miljanić OŠ. Small-molecule systems chemistry. Chem. 2017;2(4):502-24

Copyright *Author (s) 2026. Distributed under Creative Commons CC-BY 4.0*
Received*: 01-08-2026 -* ***Accepted****: 30-09-2026 -* ***Published****: 08-10-2026*

32. Kosikova T, Philp D. Exploring the emergence of complexity using synthetic replicators. Chem Soc Rev. 2017;46(23):7274-305.
33. Azcune I, Odriozola I. Aromatic disulfide crosslinks in polymer systems: Self-healing, reprocessability, recyclability and more. Eur Polym J. 2016;84:147-60.
34. Brachvogel RC, von Delius M. The dynamic covalent chemistry of esters, acetals and orthoesters. Eur J Org Chem. 2016;2016(22):3662-70.
35. Zhang Y, Barboiu M. Constitutional Dynamic Materials—Toward Natural Selection of Function. Chem Rev. 2016;116(3):809-34.
36. Lehn JM. Perspectives in chemistry—aspects of adaptive chemistry and materials. Angew Chem Int Ed. 2015;54(11):3276-89.
37. Herrmann A. Dynamic combinatorial/covalent chemistry: a tool to read, generate and modulate the bioactivity of compounds and compound mixtures. Chem Soc Rev. 2014;43(6):1899-933.
38. Hu L, Schaufelberger F, Timmer BJJ, Flos MA, Ramström O. Kirk-Othmer Encyclopedia of Chemical Technology. Hoboken: Wiley; 2014. p. 1-25.
39. Misuraca MC, Moulin E, Ruff Y, Giuseppone N. Supramolecular polymers: From structural control to functional materials. New J Chem. 2014;38(8):3336-49.
40. Wilson A, Gasparini G, Matile S. Functional systems with orthogonal photo- and redox inputs. Chem Soc Rev. 2014;43(5):1948-62.
41. Jin Y, Yu C, Denman RJ, Zhang W. Recent advances in dynamic covalent chemistry. Chem Soc Rev. 2013;42(16):6634-54.
42. Hunt RA, Otto S. Dynamic combinatorial libraries: Functional assembly in chemistry and biology. Chem Commun. 2011;47(3):847-58
43. Gasparini G, Dal Molin M, Prins LJ. Dynamic covalent chemistry: From discrete molecules to functional supramolecular systems. Eur J Org Chem. 2010;2010(23):2429-40.
44. Li Y, Wang D, Zhang L, Luo S. Redox property of enamines. J Org Chem. 2019;84(18):12071-90.
45. Kogan EA, Kuznetsov MT. Enamine compounds as potential bioactive agents: Recent advances. J Med Chem. 2019;62(10):4534-50.
46. El Basiony, N. M., Elgendy, A., Nady, H., Migahed, M. A., & Zaki, E. G. (2019). Adsorption characteristics and inhibition effect of two Schiff base compounds on corrosion of mild steel in 0.5 M HCl solution: experimental, DFT studies, and Monte Carlo simulation. *RSC advances*, *9*(19), 10473-10485.

Copyright *Author (s) 2026. Distributed under Creative Commons CC-BY 4.0*
Received*: 01-08-2026 -* ***Accepted****: 30-09-2026 -* ***Published****: 08-10-2026*